Reorganization of lipid domain distribution in giant unilamellar vesicles upon immobilization with different membrane tethers

ARTICLE *in* BIOCHIMICA ET BIOPHYSICA ACTA · JUNE 2012

Impact Factor: 4.66 · DOI: 10.1016/j.bbamem.2012.05.028 · Source: PubMed

3 AUTHORS:

Maria João Sarmento
University of Lisbon
6 PUBLICATIONS **13** CITATIONS
SEE PROFILE

Manuel Prieto
University of Lisbon
177 PUBLICATIONS **4,481** CITATIONS
SEE PROFILE

Fabio Fernandes
University of Lisbon
39 PUBLICATIONS **338** CITATIONS
SEE PROFILE

Biochimica et Biophysica Acta 1818 (2012) 2605–2615

Contents lists available at SciVerse ScienceDirect

Biochimica et Biophysica Acta

journal homepage: www.elsevier.com/locate/bbamem

Reorganization of lipid domain distribution in giant unilamellar vesicles upon immobilization with different membrane tethers

M.J. Sarmento, M. Prieto, Fábio Fernandes *

Centro de Química Física Molecular and Institute of Nanosciences and Nanotechnologies, Complexo I, Instituto Superior Técnico, Av. Rovisco Pais, 1049–001 Lisboa, Portugal

ARTICLE INFO

Article history:
Received 21 March 2012
Received in revised form 22 May 2012
Accepted 25 May 2012
Available online 1 June 2012

Keywords:
Giant unilamellar vesicles
Liposome immobilization
Membrane tether
Biotinylated lipids
Confocal microscopy
Förster resonance energy transfer

ABSTRACT

Characterization of phase coexistence in biologically relevant lipid mixtures is often carried out through confocal microscopy of giant unilamellar lipid vesicles (GUVs), loaded with fluorescent membrane probes. This last analysis is generally limited to the vesicle hemisphere further away from the coverslip, in order to avoid artifacts induced by the interaction with the solid surface, and immobilization of vesicles is in many cases required in order to carry out intensity, lifetime or single-molecule based microscopy. This is generally achieved through the use of membrane tethers adhering to a coverslip surface. Here, we aimed to determine whether GUV immobilization through membrane tethers induces changes in lipid domain distribution within liposomes displaying coexistence of lipid lamellar phases. Confocal imaging and a Förster resonance energy transfer (FRET) methodology showed that biotinylated phospholipids present significantly different membrane phase partition behavior upon protein binding, depending on the presence or absence of a linker between the lipid headgroup and the biotinyl moiety. Membrane phases enriched in a membrane tether displayed in some cases a dramatically increased affinity for the immobilization surface, effectively driving sorting of lipid domains to the adherent membrane area, and in some cases complete sequestering of a lipid phase to the interaction surface was observed. On the light of these results, we conclude that tethering of lipid membranes to protein surfaces has the potential to drastically reorganize the distribution of lipid domains, and this reorganization is solely dictated by the partition properties of the protein–tether complex.

1. Introduction

As a result of their cell-like size (10–100 μm), and spherical closed bilayer geometry, giant unilamellar vesicles (GUVs) are one of the best biomimetic membrane model in use. GUVs have been extensively used to determine phase coexistence for biologically relevant lipid mixtures [1–3], through measurement of the areas occupied by each coexisting membrane phase from intensity projections. These are created from vesicle slices obtained through confocal/biphotonic microscopy. Confocal imaging of a GUV typically requires acquisition of 20–100 confocal slices depending on the GUV size and slice *z*-separation, with the whole process taking from 10 s to several minutes. Acquisition of high quality data (with larger pixel dwell times) is extremely challenging in non-immobilized GUVs, since movements of the vesicle within the duration of the imaging procedure, result in misalignment of slices both in the *xy* and *z* directions. Although the former misalignments could potentially be corrected through alignment algorithms, correction of *z*-direction misalignment is extremely difficult. Immobilization of the vesicles virtually eliminates the problem of vesicle movement during image acquisition, and has been of great assistance in GUV imaging. Additionally, immobilization is also required for single-molecule studies such as FCS [4], as fluorescence fluctuations during signal acquisition must only be dictated by molecule diffusion and whole vesicle movements should be completely absent.

Several immobilization procedures for lipid vesicles are described in the literature. Generally they can be divided in two main groups: non-specific methods, which are driven by van der Waals and electrostatic forces or by steric entrapment, and specific tethering methods that make use of the affinity between molecules [5,6] or their capacity to form covalent bonds [7,8]. Non-specific interactions are frequently accomplished by coating a solid surface with positively charged proteins [6] or, e.g., functionalizing a polymer with an amphiphilic peptide [9]. Using a completely different strategy, Schönherr and coworkers [10] employed AFM to create patterned damages in supported lipid bilayers to which vesicles tended to adsorb. More recently, nanoparticles (NPs) were used for immobilization. Charged NPs adsorbed to the outer surface of the vesicles were observed to promote liposome immobilization in surfaces with opposite charge [11], while magnetic NPs encapsulated inside the vesicles forced the deposition through the interaction with external magnets [12]. Steric entrapment has been achieved either inside hydrogels [13] and silicon matrices [14] or, in more relaxed conditions, using microscopic picket fences [15]. To accomplish specific immobilization of the vesicles, several strategies have also been followed, including hybridization of complementary *ss*DNA [16,17]

* Corresponding author. Fax: +351 21 8464455.
E-mail address: fernandesf@ist.utl.pt (F. Fernandes).

0005-2736/$ – see front matter © 2012 Elsevier B.V. All rights reserved.
doi:10.1016/j.bbamem.2012.05.028

and interaction between selectins and lipid-anchored sialylated saccharides [18] or histidine/nickel and nitriloacetic acid [19,20]. Notwithstanding, the most common strategy relies on the affinity between biotin and avidin/streptavidin. Typically, vesicles are loaded with a trace amount of a biotinylated lipid and the immobilization is performed over an avidin-exposing surface [21–24].

Reorganization of lipid domain distribution upon vesicle immobilization through lipid tethers is of particular interest for studies aimed to thermodynamically characterize a lipid mixture exhibiting phase coexistence [25]. Here, we aimed to investigate whether immobilization of lipid vesicles through lipid tethers induces significant changes in GUVs properties, focusing on lipid domain distribution. Our results show that immobilization of lipid vesicles through lipid tethers induces changes in domain distribution and, in some conditions, with dramatic reorganization of lipid domains. Moreover, we observed that the extent of these changes largely depends on membrane composition and the partition behavior of the biotinylated lipid. Suggestions are made concerning the use of particular membrane tethers to immobilize GUVs presenting lipid phase coexistence.

2. Materials and methods

2.1. Materials

1-Palmitoyl-2-oleoyl-*sn*-glycero-3-phosphocholine (POPC), 1,2-dioleoyl-*sn*-glycero-3-phosphocholine (DOPC), 1,2-dipalmitoyl-*sn*-glycero-3-phosphocholine (DPPC), *N*-palmitoyl-D-*erythro*-sphingosylphosphorylcholine (PSM), 1,2-dioleoyl-*sn*-glycero-3-phosphoethanolamine-*N*-(cap biotinyl) (DOPE-Cap-biotin), 1,2-dipalmitoyl-*sn*-glycero-3-phosphoethanolamine-*N*-(biotinyl) (DPPE-biotin), 1,2-dipalmitoyl-*sn*-glycero-3-phosphoethanolamine-*N*-(cap biotinyl) (DPPE-Cap-biotin), 1,2-dioleoyl-*sn*-glycero-3-phosphoethanolamine-*N*-(lissamine rhodamine B sulfonyl) (DOPE-Rho) and 1,2-dipalmitoyl-*sn*-glycero-3-phosphoethanolamine-*N*-(7-nitro-2-1,3-benzoxa-diazol-4-yl) (DPPE-NBD) were obtained from Avanti Polar Lipids (Alabaster, AL). Avidin from egg white, extrAvidin-FITC conjugate and cholesterol (Chol) were from Sigma Chemical Co. (St. Louis, MO). *Trans*-parinaric acid (*t*-PnA) was from Invitrogen (Breda, The Netherlands). All organic solvents were UVASOL grade from Merck (Darmstadt, Germany).

2.2. Liposome preparation

GUVs were obtained by electroformation in Pt wires as previously described [26,27]. Briefly, lipid solutions were prepared in chloroform (from lipid stock solutions) to a final lipid concentration of 1 mM with the following compositions: DOPC:DPPC (1:1) and POPC:Chol:PSM (1:1:1), both with DPPE-NBD and DOPE-Rho in a probe/lipid ratio of 1:250 and 1:500, respectively, and with the desired amount of biotinylated lipid. For imaging of vesicles with extrAvidin-FITC, DPPE-NBD was not included in the mixture. After removal of the solvent, electroformation was performed at 58 °C during 75 min, in 1 mL of a 200 mM sucrose solution preheated at the same temperature.

Large unilamellar vesicles (LUVs) were prepared by extrusion of multilamellar vesicles. POPC and POPC:Chol:PSM (1:1:1) mixtures were prepared in chloroform to a final lipid concentration of 2 mM. Biotinylated lipids were included at a molar ratio of 1:100. The lipid solutions were dried under a N_2 flux, left in vacuum overnight and re-suspended in 1 mL of a 10 mM HEPES buffer (pH 7.4) containing 150 mM NaCl, and 3.4 mM EDTA, preheated at 50 °C. *t*-PnA was added at a 1:200 probe/lipid ratio and freeze–thaw cycles were performed to re-equilibrate and homogenize the samples. LUVs were then obtained by extrusion of the solutions at 50 °C with an Avanti Mini-Extruder (Alabaster, AL) using 100 nm pore size polycarbonate membranes.

Probe concentrations were determined spectrophotometrically, using ε(DOPE-Rho, 559 nm, chloroform) = $95\times10^3\ M^{-1}cm^{-1}$ [28], ε(DPPE-NBD, 458 nm, chloroform) = $21\times10^3\ M^{-1}cm^{-1}$ [28] and ε(*t*-PnA, 299 nm, ethanol) = $89\times10^3\ M^{-1}cm^{-1}$ [29] and ε(extrAvidin-FITC, 494 nm) = $84000\ M^{-1}cm^{-1}$ (Sigma).

2.3. Immobilization of GUVs using the avidin-biotin method

GUV solution (150 μL) was transferred to a μ-Slide from Ibidi (Munich, Germany), with or without avidin coating. Glucose solution (250 μL of 200 mM) was then added to the vesicles in order to create a density difference and stabilize a greater number of vesicles in the bottom of the chamber. For avidin coating of the slides, 200 μL of a 0.5 mg/mL avidin solution was added to each well and left overnight at room temperature. Vesicles were added to the slides after extensive washing with MilliQ water to remove excess avidin. Before measurements, slides were left immobile in the dark during 20 min, allowing time for GUVs to attach to the surface.

For the experiments with extrAvidin-FITC, no coating was performed and the glucose was replaced by the same volume of a pH 7.4 HEPES buffer (10 mM HEPES, 150 mM NaCl, 3.4 mM EDTA).

2.4. Confocal fluorescence microscopy

All measurements were performed on a Leica TCS SP5 (Leica Microsystems CMS Gmbh, Mannheim, Germany) inverted confocal microscope (DMI6000). A 63x apochromatic water immersion objective with a NA of 1.2 (Zeiss, Jena Germany) was used for all experiments, and an Argon laser was used for excitation. DPPE-NBD and DOPE-Rho excitation were achieved with the 458 and 514 nm laser lines, respectively. DPPE-NBD fluorescence was collected between 480 and 530 nm, while DOPE-Rho emission was acquired in the 530–650 nm range. For each GUV, two different sets of images were acquired: (i) a *xz* slice, where it is possible to directly observe the interaction of GUVs with the surface; (ii) *xy* slices separated by 0.4 μm along the *z*-axis, that were compiled in two GUV hemisphere projections constructed using the maximum intensity projection (MIP) method [30]. For the controls without biotinylated lipid, faster image acquisition had to be used due to vesicle motion. Surface reflexion in meridional slices was obtained by exciting and collecting emission at 458 nm.

When GUVs were incubated with extrAvidin-FITC, images were acquired sequentially in two different channels, only from the top hemisphere. Imaging of extrAvidin-FITC was performed through excitation with the 476 nm Argon laser line and emission was collected between 490 and 540 nm, while DOPE-Rho fluorescence images were obtained as described above. All analysis of confocal imaging data was carried out using ImageJ (Wayne Rasband, NIH, USA), a FIJI (http://pacific.mpi-cbg.de) plugin and homemade software developed in a Matlab environment (Mathworks, Natick, MA).

2.5. Fluorescence spectroscopy

Fluorescence measurements were carried out with a SLM-Aminco 8100 Series 2 spectrofluorimeter (Rochester, NY) with double excitation and emission monochromators (MC-400), in a right-angle geometry. The light source was a 450-W Xe arc lamp and the reference a Rhodamine B quantum counter solution. Quartz cuvettes (1×1 cm) from Hellma Analytics were used. Temperature was controlled to 25 °C by a thermostat cuvette holder and magnetic stirring was used.

t-PnA fluorescence intensities were obtained by excitation at 305 nm and fluorescence emission collection at 405 nm.

3. Theory

3.1. Determining membrane fractions of lipid phases

The presence of liquid ordered (l_o) or liquid disordered (l_d) lipid domains in GUVs can be easily identified through the use of fluorescent membrane probes. DOPE-Rho in a mixture of l_o and l_d phases is known to present a significant preference to disordered domains, with a partition coefficient ($K_{p\ lo/ld}$) = 0.28 [31]. On the other hand, DPPE-NBD has a $K_{p\ lo/ld}$ of 3.68 [31], demonstrating preference for liquid ordered domains. In the case of gel(g)-l_d lipid phase separation, DOPE-Rho is excluded from the gel phase. Simultaneous detection of both membrane probes on GUV's presenting l_o/l_d or g/l_d phase coexistence allows for discrimination of lipid phases with great accuracy (for domains with sizes much larger than the confocal resolution). From the intensity projections obtained with the two fluorescent signals it is possible to calculate the fraction of membrane area in each lipid phase. The different confocal slices present different degrees of overlap between membrane surface areas and the point spread function (PSF). As such, in a 2D projection, pixels do not correspond to identical area values. Recently, this issue was addressed through measurement of areas directly on a 3D reconstruction of the confocal data [25]. Given that a large number of vesicles were used by us to characterize each population, this effect is not expected to generate any deviation of the final average fractions of membrane area in each lipid phase, and these were determined directly from 2D projections.

In order to evaluate the influence of GUV immobilization on the lipid domain distribution, the composition of three different sections in each immobilized vesicle was determined separately: (i) top hemisphere, (ii) bottom hemisphere, and (iii) interaction surface. *xy* hemisphere projections were used to calculate the fraction of liquid ordered (or gel) phase in each hemisphere (Eq. (1)),

$$f_{lo}(\text{top}) = \frac{A_{lo}(\text{top})}{A_{lo}(\text{top}) + A_{lo}(\text{bottom})} \quad (1)$$

where A values represent the area of liquid ordered phase in the top and bottom (in contact with the surface) hemispheres. We choose to determine the fraction of a lipid phase located in the top hemisphere instead of determining the fraction of the membrane area in a particular lipid phase, since the latter quantity varies significantly between GUVs, as electroformation results in a very heterogeneous population of vesicles. In this way, by normalizing the membrane area in the l_o (or gel phase) on the top hemisphere for the total area of the GUV membrane in the same lipid phase, it is possible to detect changes in domain distribution in a heterogeneous mixture of vesicles.

Immobilization of the GUVs is expected to induce a greater disturbance of the lipid bilayer closer to the immobilization surface. However, at this level, it is not possible to directly compare areas, since curvatures are dramatically different. Making use of the acquired *xz* slices, we calculated the l_o (or gel) fraction in the interaction surface through Eq. (2):

$$f_{lo}(S_{int}) = \frac{\delta_{lo}}{S_{int}} \quad (2)$$

where S_{int} and S_{lo} are the lengths of the interaction surface and l_o phase in this surface, respectively, as shown in Fig. 1. The average $f_{lo}(S_{int})$ was also determined through Eq. (3):

$$\langle f_{lo}(S_{int}) \rangle = \frac{\sum_i^n f_{lo}(S_{int})_i}{n} \quad (3)$$

Equivalent equations were used to calculate gel phase fractions on GUVs with gel/l_d coexistence.

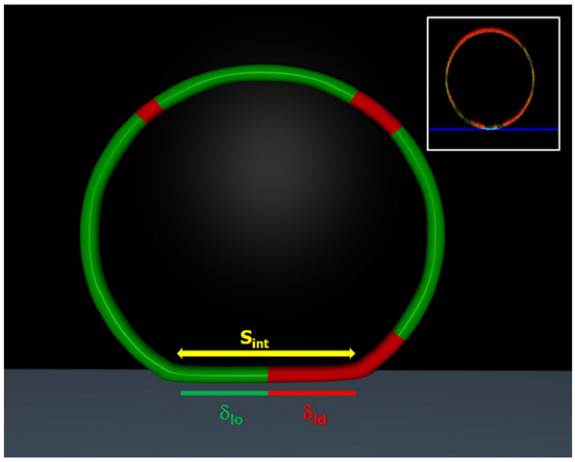

Fig. 1. Schematic representation of an immobilized GUV *xz* slice obtained from confocal microscopy. The interaction length (S_{int}) corresponds to the length of adherent membrane in the *xz* slice. δ_{lo} and δ_{ld} are the liquid ordered and liquid disordered lengths, respectively. Membrane domains are assigned on the basis of DOPE-Rho fluorescence (red), a marker for liquid disordered phases and DPPE-NBD fluorescence (green), marker of liquid ordered phases. This probe also partitions to some extent into the lipid gel phase, allowing detection of gel domains. Inset: *xz* slice of an immobilized GUV with a DOPC:DPPC 1:1 composition. DOPE-Cap-biotin was used at a ratio to total lipid of 10^{-6}. Surface reflexion in the image (blue) was obtained by exciting and collecting emission at 458 nm. The adherent membrane is defined as the surface of the vesicle which overlaps with the signal obtained from surface reflection.

3.2. Protein partition coefficient determination from confocal data

Molecular partition coefficients (K_p) between different lipid phases can be recovered from confocal microscopy studies on GUVs, given that the photophysical properties of the bound molecule (quantum yield, extinction coefficient and emission spectra) are constant in both lipid phases, and that no photoselection effects are present. In the latter case, the fluorescence of the bound molecule is independent of the orientation within each lipid phase of the GUV [32]. These requirements are not usually met by lipidic membrane probes, as their photophysical properties are normally influenced by the membrane environment, and also as a consequence of limited mobility in the membrane environment they frequently exhibit photoselectivity [32]. However, in the case of membrane anchored proteins, these criteria can be met in the cases where the fluorophore does not interact directly with the membrane environment.

Partition coefficients are defined as [33]:

$$K_p = \frac{\frac{N_1}{X_2}}{\frac{N_2}{X_2}} \quad (4)$$

where N_i the number of molecules in lipid phase i, and X_i is the molar fraction of lipid phase i. Fluorescence intensities (I_i) are directly proportional to the number of fluorescent molecules (N_i) according to Eq. (5):

$$I_i = Y \cdot N_i \quad (5)$$

where Y is a factor dependent on acquisition parameters and fluorophore photophysical properties. In case Y is identical in the two different lipid phases, and specific molecular areas in the coexistent phases are considered equal, Eq. (4) can be converted to:

$$K_p = \frac{\frac{\sum I_1}{A_1}}{\frac{\sum I_2}{A_2}} = \frac{\langle I_1 \rangle}{\langle I_2 \rangle} \quad (6)$$

where A_i is the total area occupied by lipid phase i, and I_i is the fluorescence intensity per pixel in the lipid phase i (after correction for dark counts).

3.3. Partition coefficient determination from FRET data

FRET efficiency, E, was calculated from the ratio of intensity of donor steady-state emission in the presence (I_{DA}) and absence (I_D) of the acceptor:

$$E = 1 - \frac{I_{DA}}{I_D} \tag{7}$$

Alternatively, E can also be calculated from the ratio of the integrals of the time-resolved donor emission in the presence ($i_{DA}(t)$) and absence ($i_D(t)$) of the acceptor:

$$E = 1 - \frac{\int_0^\infty i_{DA}(t)}{\int_0^\infty i_D(t)} \tag{8}$$

For a nearly two dimensional system (at the FRET scale) such as a membrane bilayer, where FRET donors and acceptors species are found randomly distributed in well defined planes, the donor decay law is described by [34],

$$i_{DA}(t) = i_D(t)\rho_{FRET} \tag{9}$$

$$\rho_{FRET} = \exp\left\{-2\sigma_A \pi l^2 \int_0^1 \frac{1-\exp\left(-tb^3\alpha^6\right)}{\alpha^3} d\alpha\right\} \tag{10}$$

$$b = \left(R_0^2/l\right)^2 \tau_D^{-\frac{1}{3}} \tag{11}$$

where σ_A is the acceptor density in each bilayer leaflet, l is the distance between the plane of donors and acceptors, R_0 is the Förster distance for the donor/acceptor FRET pair, and τ_D is the donor lifetime. In Eq. (10), it is assumed that no acceptor exclusion around the donor exists. The value of R_0 was calculated independently based on spectroscopic data according to:

$$R_0 = 0.2108\left(n^{-4}\Phi_D K^2 J\right)^{\left(\frac{1}{6}\right)} \tag{12}$$

$$J = \int f_D(\lambda)\varepsilon_A(\lambda)^4 d\lambda \tag{13}$$

where Φ_D is the quantum yield in the absence of acceptors, κ^2 the orientation factor, n the refractive index of the medium where FRET takes place, λ the wavelength, f_D the normalized emission spectra of the donor and ε_A is the molar absorption coefficient of the acceptor. The numeric factor in Eq. (12) assumes nm units for the wavelength and Å units for R_0. Here, the κ^2 value was considered to be 2/3, corresponding to the isotropic dynamic regime. This is a reasonable approximation given the long excited state lifetime of the donor used in this study, the fluidity of both l_d and l_o phases, and the fact that the acceptors are located in a mobile protein bound to the membrane [35]. In this case, the acceptor experiences motion due to dynamics at both global protein and local levels. Additionally, the R_0 dependence on $(k^2)^{1/6}$ strongly mitigates noncritical uncertainties in the value of k^2 [36].

When the distance between the plane of randomly distributed donors and acceptors in the membrane is known, it is possible to theoretically determine FRET efficiencies from Eqs. (9)–(13). In the case of lipid phase coexistence with formation of domains in the lipid bilayer, and the two lipid phases presenting different acceptor concentrations, then two populations of donor molecules with two different quantum yields will coexist. Additionally, in case the donor quantum yield is also different for each phase in the absence of acceptors, and the average domain size is significantly larger than the R_0 value (so that FRET between species in different lipid phases is negligible), the obtained donor decay can be described by:

$$i_{DA}(t) = \sum_i f(i) i_D^i(t) \cdot \rho_{FRET}^i(t) \tag{14}$$

where f(i) is the fraction of donor molecules in lipid phase i, i_D^i(t) is the donor decay in i, and ρ_{FRET}^i is the FRET contribution to the decay of donors in the lipid phase i. The latter parameter is determined from Eqs. (10)–(13) taking into account the differences in concentration of acceptors (σ_A^i), and the quantum yields of the donor (Φ_D^i). In this way, when l, f(i) and Φ_D^i values are know, it is possible to recover the acceptor concentration (σ_A in Eq. (10)) in each lipid phase from the experimentally obtained FRET efficiencies. This allows the determination of its phase partition coefficient, K_p, according to Eq. (4).

4. Results

4.1. Partition of biotinylated lipids to different lipid phases

4.1.1. From microscopy intensity data

In order to directly observe the binding of extrAvidin (a modified form of avidin), to membrane-incorporated PE-biotin molecules, we

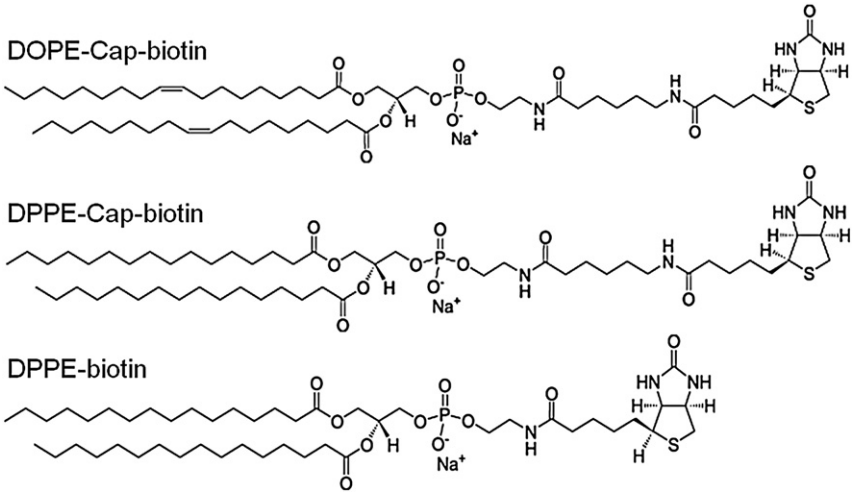

Fig. 2. Structure of biotinylated lipids.

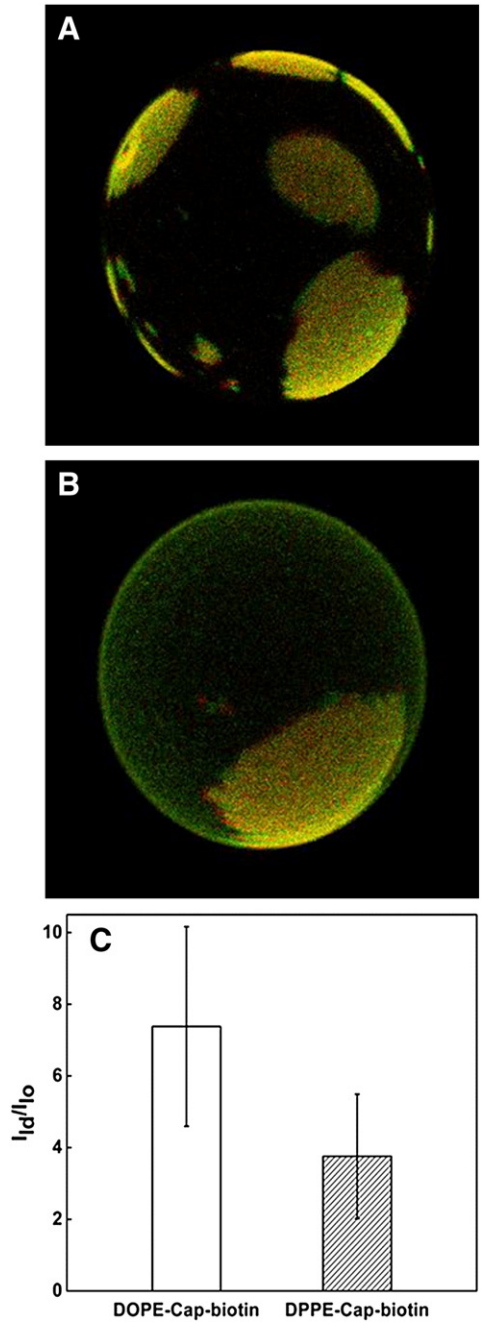

Fig. 3. Partition of complexes of biotinylated lipid and extrAvidin to different lipid phases as seen from confocal data. Non-immobilized GUVs (composition POPC:Chol:PSM 1:1:1) were labeled with DOPE-Rho at a ratio to total lipid of 1:500. Biotinylated lipid was included at a ratio to total lipid of 1:100 and extrAvidin-FITC was added to the vesicles at 0.4 μM. The fluorescence from extrAvidin-FITC (green) and DOPE-Rho (red) was sequentially collected and projections for the top hemisphere of the vesicles are shown for GUVs loaded with DOPE-Cap-biotin (A) and DPPE-Cap-biotin (B). The ratio of average intensities at the equator for each lipid phase depends on the biotinylated lipid, denoting distinct partition properties (C).

prepared GUVs of POPC:Chol:PSM (1:1:1) composition, presenting l_o/l_d phase coexistence. DOPE-Rho and each one of the studied biotinylated lipids (Fig. 2) were included in a fluorescent probe:total lipid and PE-biotin:total lipid ratios of 1:500 and 1:100 respectively. After incubating the vesicles with 0.4 μM of extrAvidin-FITC, confocal images from both fluorophores were acquired as presented in Fig. 3. Fluorescence intensity values of extrAvidin-FITC bound to PE-biotin molecules in each lipid phase were determined using a digital filter mask obtained from the DOPE-Rho channel, whose pixels correspond to the l_d phase. From the observation of the confocal projections, a higher FITC fluorescence intensity is observed in the l_d phase and average I_{ld}/I_{lo} ratio values (intensities are determined after background correction) for GUVs containing DOPE-Cap-biotin and DPPE-Cap-biotin are presented in Fig. 3C. It is clear that both biotinylated lipids have preference for the more disordered phase, and from this data, we estimated $K_{p\ ld/lo}$ values of 7.4 ± 2.8 and 3.8 ± 1.8 for DOPE-Cap-biotin and DPPE-Cap-biotin respectively.

The error associated with these partition coefficients is likely to be due to the presence of a heterogeneous population of vesicles, as this is common for GUVs with complex compositions prepared by electroformation. Nevertheless, given that the variation in $K_{p\ ld/lo}$ values was limited, we can assume that the degree of phase composition heterogeneity was not high enough to change partition of extrAvidin-FITC to a significant extent. Also, since $K_{p\ ld/lo}$ values recovered from GUVs do not correlate with the fraction of *ld* phase in the vesicles, the selection of GUVs displaying phase coexistence did not create a significant bias in lipid phase composition in this lipid mixture.

GUVs incorporating DPPE-biotin resulted in significantly lower amounts of extrAvidin binding, precluding the application of this methodology for this lipid.

4.1.2. From FRET methodologies

Since it was not possible to recover a partition coefficient for DPPE-biotin through microscopy, we employed the FRET methodology described in the Theory section. *t*-PnA and extrAvidin-FITC were used as the donor and as the acceptor species respectively (Fig. 4A and B). *t*-PnA intercalates between lipid chains and its quantum yield is very sensitive to the formation of more rigid phases [37]. Given that R_0 is dependent on the donor quantum yield (Eq. (12)), FRET efficiencies are slightly different depending on the environment where the energy transfer takes place. We determined R_0 values for the *t*-PnA/FITC FRET pair of $R_0 = 24$ Å in l_d and $R_0 = 29$ Å in the l_o phase. Since the partition coefficient of *t*-PnA in this l_o/l_d mixture is close to 1 [31], the distribution of the donor species is assumed to be random, and the fraction of donor in each phase is given by the membrane fraction of that phase (which is known from the phase diagram). An important requirement for this type of analysis is that no energy transfer occurs from donors in one lipid phase to acceptors in the other, and this condition is only met if the average lipid domain size is a few times larger than the Förster radius [38]. As can be observed from the confocal data, the average domain size observed for the 1:1:1 POPC:Chol:PSM far exceeds the *t*-PnA/FITC R_0 of 24–29 Å, and this analysis could be applied to this system.

The modeling used for the FRET analysis is described in Fig. 4A. The acceptors are all considered to be located in the geometrical center of the protein, while the distances between *t*-PnA (located on the two membrane leaflets) and this acceptor plane (l_1 and l_2) were determined on the basis of the known location of the donor in the membrane [39] and geometrical considerations on the structure of avidin [40]. Upon addition of extrAvidin-FITC to preformed liposomes, the protein is exclusively bound to the outer leaflet of the bilayer. Since not all the acceptor bounds to the membrane, the acceptor concentration was recovered from FRET experiments on POPC liposomes with 1% biotinylated lipid, assuming a random distribution of protein (Fig. 4C). In fact, acceptors are not strictly randomly distributed as each protein is labeled at 3–5 positions, and as such, acceptor concentrations are slightly underestimated. Notwithstanding, these clusters of 3–5 acceptors are themselves apparently randomly distributed as seen from confocal data. As a control, we performed the same analysis for the two biotinylated lipids for which partition coefficients had already been recovered through confocal microscopy. The partition coefficient values recovered from this FRET methodology in 1:1:1 POPC:Chol:PSM, were similar to the values obtained from the confocal data ($K_{p\ ld/lo} = 5.6$ for DOPE-Cap-biotin and $K_{p\ ld/lo} = 4.8$

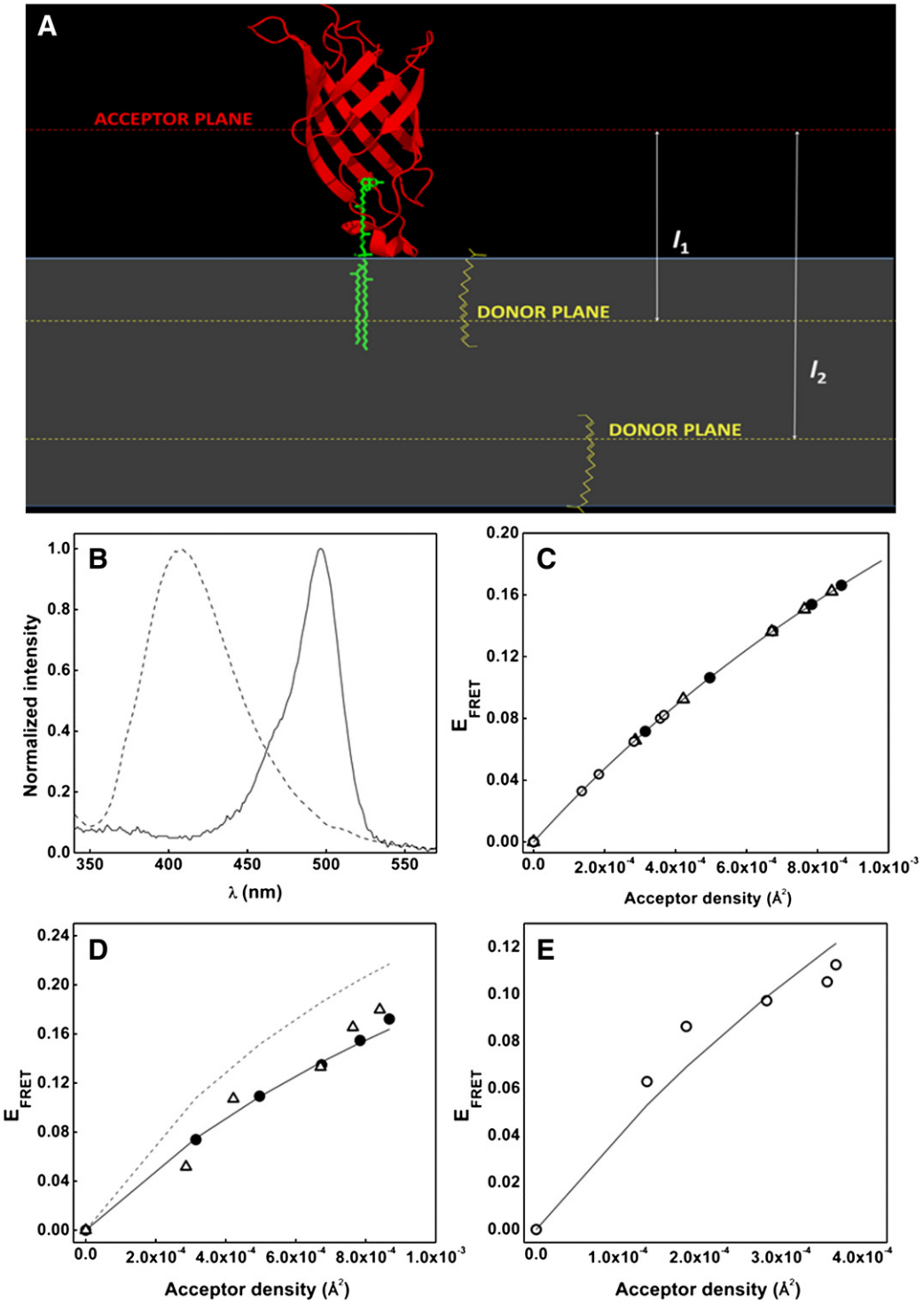

Fig. 4. Membrane phase partition of complexes of DPPE-Cap-biotin and extrAvidin measured from FRET methodology. (A) Modeling used for the FRET analysis. The acceptors are considered to be located in the plane crossing the geometric center of the protein, and *t*-PnA is located deep in the membrane [39]. The position of the acceptor plane was determined on the basis of geometrical considerations of the structure of avidin [40]. Binding of acceptors only occurs in the outer layer of the membrane. (B) Fluorescence emission spectra of *t*-PnA (——-) and absorption spectra of FITC (—). Extensive spectral overlap is present, and the R_0 for FRET was determined to be 24 Å in l_d and 29 Å in the liquid ordered phase. (C) Experimental FRET efficiencies for the *t*-PnA/FITC FRET pair in POPC liposomes with 1% biotinylated lipid. Since extrAvidin-FITC was not completely bound to the membrane in the conditions of these experiments, acceptor concentrations were determined from FRET efficiencies (E) measured in POPC liposomes assuming a random distribution of protein in the bilayer according to Eq. (10). FITC concentrations were then assumed to be identical for the PC:Chol:PSM lipid mixture. (•) DOPE-Cap-biotin; (Δ) DPPE-Cap-biotin; (○) DPPE-biotin; (—) theoretical expectation for FRET efficiencies for a planar and random distribution of acceptors separated from two planes of donors by 30 and 50 Å respectively, with $R_0 = 24$ Å. (D) Experimental FRET efficiencies for the *t*-PnA/FITC FRET pair in PC:PSM:Chol 1:1:1 liposomes with l_o/l_d phase coexistence, loaded with DOPE-Cap-biotin (•) or DPPE-Cap-biotin (Δ). Expected E values for $K_{p\ ld/lo} = 1$ for the biotinylated lipid:extrAvidin complex (——-), and the result of fitting Eq. (14) to the data obtained with DOPE-Cap-biotin (—) are plotted. $K_{p\ ld/lo} = 5.6$ was recovered for DOPE-Cap-biotin. (E) FRET efficiencies obtained in the same lipid mixture loaded with DPPE-biotin (○) and the result of fitting Eq. (14) to the data (—). $K_{p\ ld/lo} = 0.93$ was recovered for DPPE-biotin, denoting a slight preference for partition to liquid ordered domains.

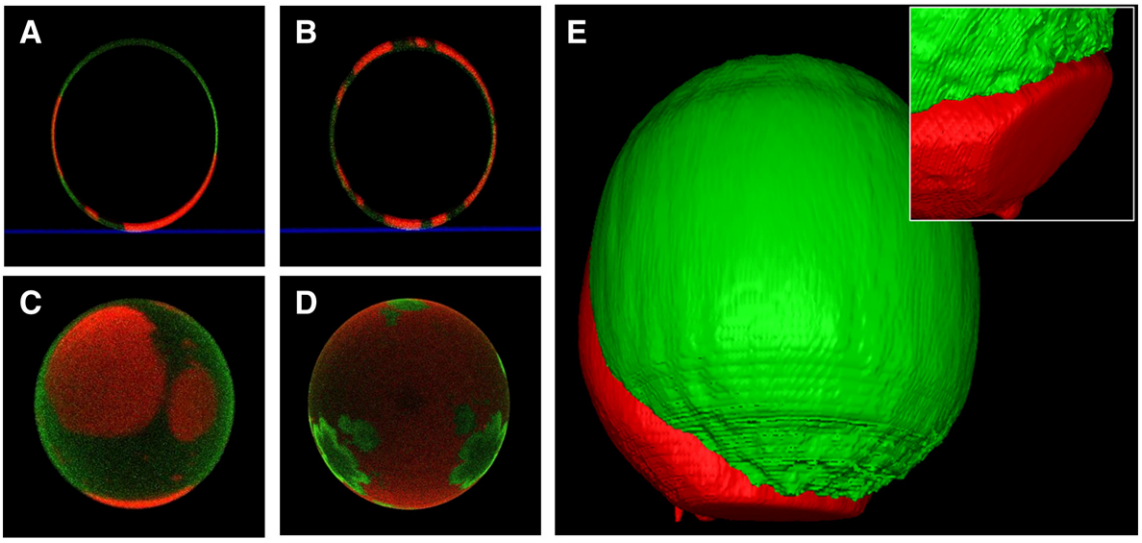

Fig. 5. Redistribution of lipid domains in GUVs upon immobilization with DOPE-Cap-biotin. Immobilized GUVs were labeled with DOPE-Rho (red) and DPPE-NBD (green) at a ratio to total lipid of 1:500 and 1:250 respectively. DOPE-Cap-biotin was included at a ratio to total lipid of 10^{-6}. After electroformation, GUVs were added to avidin-coated slides to achieve immobilization. *xz* slices are shown for POPC:Chol:PSM 1:1:1 (A) and DOPC:DPPC 1:1 (B) mixtures. Maximum intensity projections of hemispheres from GUVs composed of POPC:Chol:PSM 1:1:1 (C) and DOPC:DPPC 1:1 (D) are also shown. A three dimensional representation of a GUV exhibiting l_o/l_d phase coexistence and showing high selectivity of surface adherent area for the liquid disordered phase was obtained (E). Inset: Detail of membrane area adherent to the slide surface with full coverage by a l_d domain.

for DPPE-Cap-biotin, Fig. 4D), validating the methodology and the geometric assumptions of the model.

The $K_{p\ ld/lo}$ for DPPE-biotin obtained from the FRET data was 0.93 (Fig. 4E), reflecting a minor preference for the cholesterol enriched phase. Apparently, the absence of a flexible spacer in the phospholipid structure results in a more effective packing of the phospholipid inside the more ordered phase. It is clear that the presence of the Cap biotinyl group in the phospholipid headgroup does not have a strong effect on the partition behavior of unsaturated lipids (DOPE) in this lipid mixture, as the partition coefficient of DOPE-Cap-biotin is very similar to the value found for DOPC ($K_{p\ ld/lo}$ ~6.7) [41]. However, the Cap biotinyl group dramatically decreases partition to the liquid ordered phase of saturated lipids (DPPE). In fact, while saturated lipids are commonly found enriched in the liquid ordered phase, DPPE-Cap-biotin presents lower affinity for l_o than the fluorescent probe used in this study to label l_d domains. Manley and co-workers obtained $K_{p\ ld/lo} = 5.9$ for this biotinylated lipid on a 50:30:20 DOPC:Chol:SM mixture, suggesting that even higher DPPE-Cap-biotin segregation should occur on the more fluid l_d phase present in this mixture [42].

4.2. Influence of PE-biotin/avidin immobilization on lipid phase distribution inside GUVs

In order to investigate the influence of the immobilization method in the lipid phase distribution in GUVs, we performed confocal fluorescence microscopy in vesicles with phase coexistence and now selecting two different biotinylated lipids (DOPE-Cap-biotin and DPPE-biotin). GUVs of 1:1 DOPC:DPPC (presenting gel/l_d phase coexistence at 23 °C) and 1:1:1 POPC:Chol:PSM (presenting l_o/l_d phase coexistence at 23 °C) were obtained. At this temperature, ~25% gel is expected for 1:1 DOPC/DPPC and ~80% l_o for 1:1:1 POPC:Chol:PSM [43,44]. The electroformation technique is known for generating very heterogeneous populations of vesicles, and for this reason, measurements for each condition included data from different electroformations [45]. Moreover, we only acquired images of GUVs with phase coexistence, inducing a minor bias for vesicles with higher amounts of the less representative lipid phase. Only ratios of membrane fraction in the l_o phase (and gel phase) in each hemisphere to total membrane fraction in the GUV (Eq. (1)) were compared, in order to prevent observation of artifacts induced by a biased vesicle population. In the absence of domain reorganization, a value of 50% is expected for $<f_{lo}(\text{top})>$ (and $<f_g(\text{top})>$), while $<f_{lo}(S_{int})>$ and $<f_g(S_{int})>$ are expected to be ~80% and ~25%, respectively.

Upon directly monitoring the degree of vesicle movement and stability under the microscope, we established that a PE-biotin:lipid ratio of $1{:}10^6$ would be enough to immobilize the GUVs to a significant extent, while higher concentrations of biotinylated lipid led to an excessive degree of adsorption and increased rates of vesicle collapse. Moreover, we observed that at this low ratio, the immobilization procedure did not significantly change the curvature of the vesicles, with the exception of the adsorbed membrane area (results not shown). Controls without any biotinylated lipid, in the presence or absence of an avidin-coated surface, were also performed. DOPE-Rho and DPPE-NBD were used as lipid phase reporters, and membrane areas with DOPE-Rho fluorescence were considered to correspond to liquid disordered phases, while brighter DPPE-NBD membrane patches corresponded to the liquid ordered phase in our analysis. Some examples of the obtained *xz* slices and hemisphere projections are shown in Fig. 5. f_{lo} values for the adsorbed surface as well as for the hemispheres were recovered as described in the Theory section and results are shown in Fig. 6.

The domain distribution was also dependent on the surface composition, even without immobilization. More specifically, interaction with an avidin-coated surface alone, induced enrichment of l_d phase on the membrane area in contact with the avidin-coated surface ($<f_{lo}(S_{int})> = 49\%$), while in the absence of avidin, the fraction of l_o phase in the same area (98%) far exceeded the thermodynamic expectation from the phase diagrams (~80%) [44], denoting a redistribution of domains in the lipid vesicle upon surface adhesion. Possibly, since interaction of membranes with solid surfaces is known to reduce bilayer dynamics [46], interaction of the vesicles with the surface may promote segregation of the more ordered l_o domain to the adherent membrane area. Nevertheless, these changes in the distribution of lipid domains were restricted to the interaction surface, as the recovered $<f_{lo}(\text{top})>$ values were close to 50%.

When immobilization was performed with DOPE-Cap-biotin, dramatic changes in domain distribution were observed ($<f_{lo}(\text{top})$

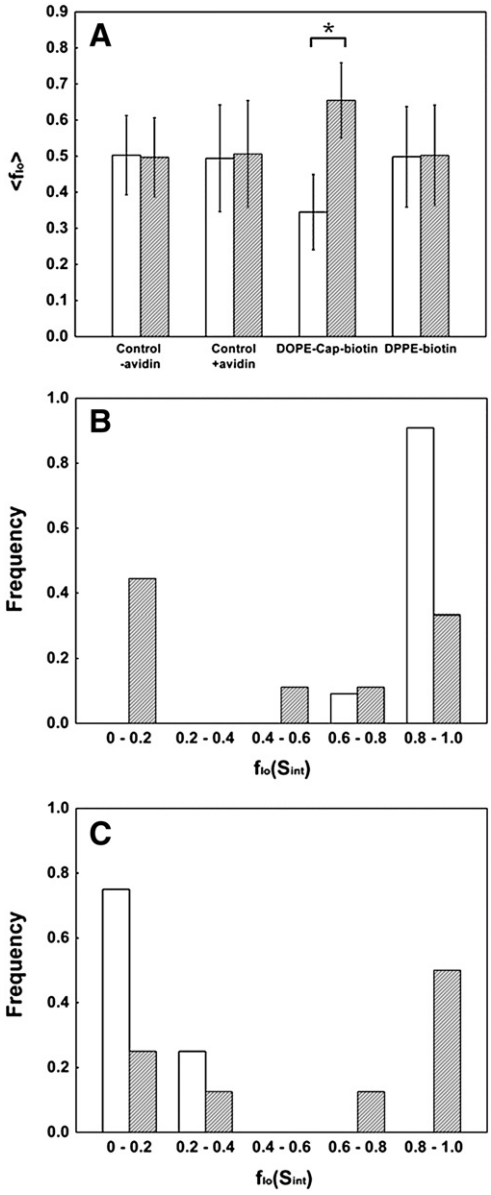

Fig. 6. Fractions of liquid ordered phase in immobilized POPC:Chol:PSM 1:1:1 GUV hemispheres and adherent membrane section. (A) $<f_{lo}>$ values are shown for the top (filled) and bottom (open) hemispheres. Absence of lipid domain reorganization upon immobilization is expected to result in a value of 0.5 on the GUV's ensemble average. Control experiments performed in the absence of biotinylated lipid with or without avidin have no effect in the average distribution of lipid domains within each GUV. Vesicle immobilization with the unsaturated DOPE-Cap-biotin results in a very significant enrichment of the bottom immobilized hemisphere in l_d domains ($p<0.01$). Immobilization with DPPE-biotin did not influence average domain distribution. (B) Histogram for the distribution of $f_{lo}(S_{int})$ values in the absence of a membrane tether, with (filled) and without (open) avidin in the interaction surface. Interaction with the protein surface induces segregation of l_d domains to the adherent membrane area ($<f_{lo}(S_{int})>=49\%$), while in the absence of protein coating clear preference for l_o interaction was detected ($<f_{lo}(S_{int})>=98\%$). $<f_{lo}(S_{int})>$ values are not shown in the figure. (C) Histogram for the distribution of $f_{lo}(S_{int})$ values in the presence of a membrane tether. Results are shown for the unsaturated DOPE-Cap-biotin (open) and the saturated DPPE-biotin (filled). Immobilization with DOPE-Cap-biotin results in a drastic change in lipid composition of the surface adherent membrane ($<f_{lo}(S_{int})>=8\%$), while GUVs immobilized with DPPE-biotin presented a $<f_{lo}(S_{int})>$ value close to the control without tether (56%). Analysis of lipid domain reorganization upon surface interaction was performed for 9–12 GUVs in each condition, and only fully immobile vesicles were considered for GUVs loaded with DOPE-Cap-biotin and DPPE-biotin.

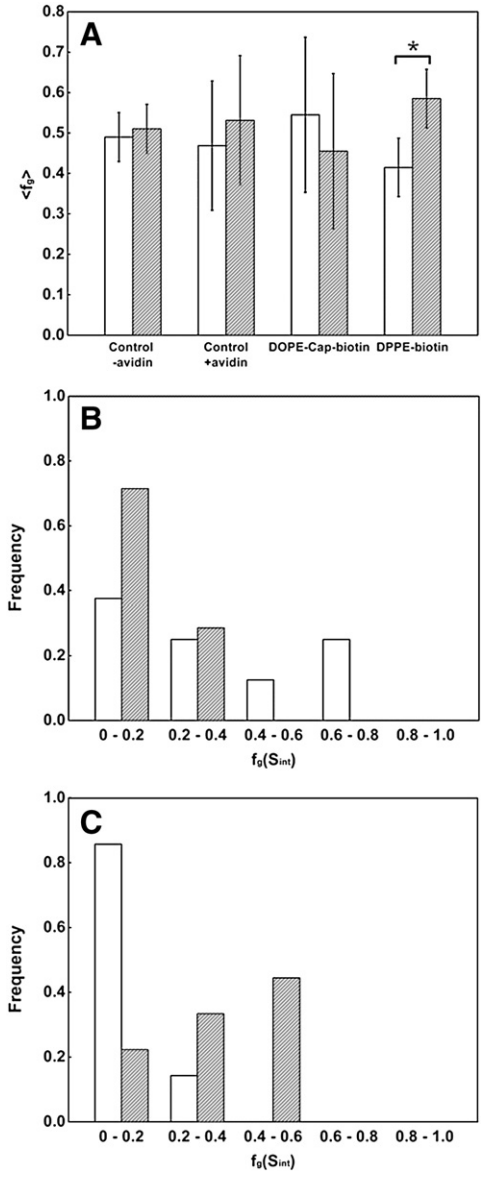

Fig. 7. Fractions of liquid ordered phase in immobilized DOPC:DPPC 1:1 GUV hemispheres and adherent membrane section. (A) $<f_g>$ values are shown for the top (filled) and bottom (open) hemispheres. GUVs in the absence of biotinylated lipid, with or without avidin surface coating have almost no difference in averaged lipid composition in the 2 hemispheres. Vesicles immobilized with the unsaturated DOPE-Cap-biotin also presented closer lipid composition in each hemisphere, while for the saturated DPPE-biotin, the bottom hemisphere is slightly enriched in the fluid phase ($p<0.01$). (B) Histogram for the distribution of $f_g(S_{int})$ values in the absence of a membrane tether, with (filled) and without (open) avidin in the interaction surface. Once again, interaction with the protein surface induced segregation of l_d domains to the adherent membrane area ($<f_g(S_{int})>=6\%$), while in the absence of protein coating no domain reorganization is observed ($<f_g(S_{int})>=31\%$). $<f_g(S_{int})>$ values are not shown in the figure. (C) Histogram for the distribution of $f_g(S_{int})$ values in the presence of a membrane tether. Results are shown for the unsaturated DOPE-Cap-biotin (open) and the saturated DPPE-biotin (filled). Immobilization with DOPE-Cap-biotin results in sequestration of fluid domains to the interaction surface ($<f_g(S_{int})>=3\%$), while immobilization with the saturated lipid tether induced a minor enrichment in the gel phase ($<f_g(S_{int})>=34\%$). Analysis of lipid domain reorganization upon surface interaction was performed for 9–11 GUVs in each condition, and only fully immobile vesicles were considered for GUVs loaded with DOPE-Cap-biotin and DPPE-biotin.

$>=66\%$), particularly in the membrane area adhering to the immobilization surface, where the average fraction of l_o ($<f_{lo}(S_{int})>$) is 8% (Fig. 6).

A three dimensional reconstruction of a representative vesicle immobilized with DOPE-Cap-biotin and presenting domain reorganization is shown on Fig. 5. The selectivity of the avidin-coated surface

for liquid disordered domains was dependent on the concentration of biotinylated lipid, since upon a 10 times increase in the concentration of DOPE-Cap-biotin, $<f_{lo}(S_{int})>$ increased to 56%, reflecting significantly less domain redistribution (results not shown). However, this concentration of biotinylated lipid resulted in a much higher rate of GUV collapse.

Immobilization of GUVs with DPPE-biotin resulted in a $<f_{lo}(S_{int})>$ of 56% (Fig. 6), a minor increase in the affinity of the liquid ordered phase for the coated surface when compared with the value recovered for the surface coated with avidin in the absence of the biotinylated lipid. Importantly, this low level of enrichment did not change the average composition of the hemispheres (Fig. 6A).

From the data in Fig. 6, it is also clear that lipid domain boundaries are almost never observed in the interaction surface of GUVs with l_o/l_d domain coexistence, both for immobilized and non-immobilized vesicles. In fact, either l_o or l_d domains often spanned the entire adhesion surface, and the boundaries of these domains were in most cases found in the edges of this area (Fig. 5A and E), reflecting the significant differences in surface affinities of each phase.

The same methodology was applied to the DOPC/DPPC 1:1 lipid mixture and results are shown in Fig. 7. Once again, DOPE-Rho was used as a reporter of liquid disordered phase, while some extent of DPPE-NBD partition into gel domains allowed their visualization. Fractions of gel phase were determined as described for liquid ordered phase in Eqs. (1) and (2). In the absence of any immobilization procedure (non-coated surface), the composition of the interaction surface is highly variant, with an average fraction of gel phase ($<f_g(S_{int})>$) of 31% suggesting that the contact with the surface is not restricted or phase dependent, as $<f_g(S_{int})>$ is very similar to the expected value for a randomized distribution of gel domains within the GUV (25%) [43]. When the avidin-coated surface is used (without biotinylated lipid), GUVs interact with the surface preferentially through the fluid phase with an $<f_g(S_{int})> = 6\%$. Despite this, the average composition of the hemispheres remained unaltered for both control populations (Fig. 7A).

When vesicles were immobilized with DOPE-Cap-biotin, interaction with the surface also strongly favored the fluid phase ($<f_g(S_{int})> = 3\%$), suggesting a preferential partition of the lipid to this membrane environment (Fig. 7C). In this case, the extremely low density of biotinylated lipids in the gel domains would dramatically decrease the probability of an effective contact with the avidin surface through DOPE-Cap-biotin molecules located in this phase. However, this effect did not extend to the hemisphere composition (Fig. 7A), possibly as a result of the smaller domain sizes observed in a gel/fluid lipid phase coexistence. In this way, lipid domain reorganization in immobilized GUVs presenting domain sizes comparable to the interaction surfaces, is almost entirely restricted to the adherent membrane area. Additionally, since in this mixture, the I_d phase comprises most of the bilayer (75%) [43], selectivity for surface interaction through this lipid phase is much less likely to induce a significant reorganization of lipid domains inside the GUVs.

On the other hand, immobilization resorting to DPPE-biotin resulted in a $<f_g(S_{int})>$ value of 34%. Additionally, in all vesicles studied for this case, a gel/fluid domain boundary was always present in the interaction surface. It is possible that DPPE-biotin upon binding to the avidin surface, presents preferential partition to the gel/fluid interface, explaining the increased fraction of gel phase in the adherent membrane area. A similar behavior is presented by DPPE-NBD as can be seen from Fig. 5D, with a noticeable increased intensity within gel/fluid domain boundaries. However, the average f_g in the hemisphere interacting with the coated surface (bottom hemisphere) is slightly lower than the value obtained for the top hemisphere (Fig. 7A). This could be rationalized on the basis of accumulation of this biotinylated lipid in the domain boundaries, so the local concentration of the membrane tether will increase several fold, in this way increasing the rate of vesicle collapse. In this case, GUVs with a higher percentage of gel domains in the bottom hemisphere are less stable than vesicles with a higher percentage of fluid phase in this area, and the distribution of GUVs would be somewhat biased towards lower gel fractions in the interacting hemisphere.

5. Discussion

The results from extrAvidin-FITC distribution on GUVs under phase coexistence clearly demonstrate that the partition coefficient of biotinylated phospholipids for the biologically relevant l_o/l_d phase coexistence diverges significantly from unity, denoting in some cases a dramatic preference for interaction with liquid disordered phases. The $K_{p\ ld/lo}$ recovered for DOPE-Cap-Biotin ($K_{p\ ld/lo} = 7.4 \pm 2.8$) is even larger than the partition coefficient of DOPE-Rho ($K_{p\ ld/lo} = 3.6$ [31]), while DPPE-Cap-biotin presents a $K_{p\ ld/lo} = 3.8 \pm 1.8$. On the other hand, using a FRET methodology, DPPE-biotin was shown to have some preference for the liquid ordered phase, with a $K_{p\ ld/lo} = 0.93$.

Interestingly, when a linker was included in the biotinylated lipids, partition to the liquid disordered phase was significantly increased when compared with the biotinylated lipid without the linker. This is probably a result of increased dynamics in the protein-lipid complex when a linker is present, possibly the same condition that considerably increases protein:PE-biotin binding affinity. In these conditions, incorporation in the more rigid liquid ordered environment is much less efficient, while the less flexible avidin:biotin-PE complex in the absence of a linker, presents more efficient packing in this phase. It should be noted that the partition coefficients determined here, correspond to the protein bound form of the lipid, and this is likely to be different from the partition coefficient of the freely diffusing phospholipid. In fact, it is known that upon binding to avidin in a lipid membrane, biotin-PEs are vertically displaced out of the membrane to some extent [47], and this new conformation of the lipid in the membrane will induce different interactions with the surrounding lipids. As a result of the bivalent character of avidin-biotin interaction with membrane surfaces (only two monomers in the avidin tetramer face the same surface upon binding), a formation of 2:1 biotin-PEs:avidin complexes is expected as biotinylated lipids were present in large excess of protein concentrations, and this is likely to create additional lipid diffusion constraints after protein binding. Many palmitoylated proteins are known to partition to lipid rafts [48], and in the absence of a linker, the complex of avidin with two biotinylated lipids such as DPPE, share some properties with palmitoylated proteins, as the protein exhibits some preference for liquid ordered membranes. The difference in behavior of the two biotinylated lipids with palmitoylated acyl-chains is in agreement with a report showing that liquid ordered partition of small palmitoylated peptides was extremely dependent on the peptide structure, with nearly identical peptides presenting 10 fold difference in partition coefficients to the liquid ordered phase, depending on the position of the lipid modification [49].

In order to prevent an excess of membrane adhesion to the surface and consequently vesicle collapse, the immobilization of GUVs in avidin or streptavidin-coated surfaces is normally performed with extremely low concentrations of biotinylated lipid ($\sim 10^{-6}$ ratio to total lipid content). Such low concentrations are not expected to disturb membrane phase properties in any way, and have been widely used in studies of model membranes which require immobilization. Nevertheless, since different biotinylated lipids present different membrane partition properties as seen here, their use in immobilization of membrane model systems has the potential to drive changes in lipid domain distribution, as coexisting phases will present different levels of enrichment for the lipid driving immobilization.

The effect of the different partition coefficients observed for these membrane tethers on the distribution of membrane domains in GUVs was studied here through confocal imaging for a biotinylated lipid with high affinity for the l_d phase (DOPE-Cap-biotin) and a biotinylated

lipid with modest affinity for the l_o phase (DPPE-biotin). We showed that when using an immobilization driving lipid with a strong preference for a lipid phase comprising a small fraction of the membrane, there is a dramatic reorganization of the distribution of lipid domains upon interaction with the immobilizing surface. DOPE-Cap-biotin almost completely excluded liquid ordered domains from the interaction surface in POPC:Chol:PSM 1:1:1 GUVs, even though this lipid phase comprises around 80% of the total membrane fraction area. Given the typically large sizes for domains observed in this lipid mixture, this selectivity induced very significant changes in the lipid phase composition of both GUV hemispheres. When a single large l_d domain was present in the vesicle, immobilization with DOPE-Cap-biotin entrapped this domain in the bottom hemisphere, virtually depriving the top hemisphere of liquid disordered phase, even though l_d corresponded still to a significant fraction of the membrane (Fig. 5E). When the unsaturated lipid tether was included in the lipid mixture at a ratio to total lipid of 10^{-5}, 10 times higher than the concentration used in the other studies, selectivity for specific membrane phases was no longer observed, suggesting that the membrane tether is already at a saturating concentration. However, this concentration increased significantly the rate of GUV collapse in the avidin-coated surface.

As a result of a $K_{p\ ld/lo}$ close to unity, DPPE-biotin did not induce very significant changes in lipid domain distribution on GUVs composed of POPC:Chol:PSM 1:1:1 upon immobilization. The fraction of l_o phase in the interaction surface was only slightly increased relative to the value obtained in the absence of the membrane tether, reflecting the minor preference of the molecule for the liquid ordered environment.

On another lipid system with gel and l_d lipid domains, reorganization of lipid domains within the vesicles is largely limited to the adherent membrane area, probably as a consequence of the smaller domain areas. DOPE-Cap-biotin promotes, as expected, immobilization through the fluid phase, while DPPE-biotin apparently partitions to the interfaces of gel/fluid domains, increasing slightly the fraction of gel phase in the immobilized surface. Partition of this lipid to the gel domains is unlikely, since molecules with bulky headgroups are known to be segregated from the gel phase as a consequence of tight lipid packing [50].

Surprisingly, considerable changes in the lipid composition of the adherent membrane were observed in the absence of immobilization. GUVs on uncoated surfaces interacted with the support almost entirely through l_o domains, while more l_d than expected was present in the case of coated surfaces. For lipid mixtures presenting gel/fluid coexistence, gel was also largely excluded of the membrane adherent area. These results reflect the energetic penalty associated with a more ordered phase interacting with the non-smooth protein surface.

Although this study focused on biotinylated phospholipids, results presented here are presumably extensive to other type of immobilizations using lipid tethers, such as lipidated *ss*DNA. It is clear that differential partition of lipid tethers even at the extremely low ratio to total lipid of 10^{-6}, is able to modulate the organization of lipid domains within lipid vesicles. Studies aimed to thermodynamically characterize a particular lipid mixture exhibiting phase coexistence through GUV microscopy, often rely on sole characterization of the top hemisphere as a way to avoid artifacts originating from the interaction with the surface. Considering the results presented here, this selective analysis is not able to fully characterize lipid phase coexistence, and is particularly prone to artifacts when lipid domain sizes are comparable or larger than the adhesion surface. In order to apply such methodology, it is necessary to carefully characterize the membrane partition properties of the chosen membrane tether, particularly for lipid mixtures exhibiting lipid domains of significant area.

Reconstituted actin skeleton has been shown to determine the localization of membrane domains in GUVs through interaction with PIP2-N-WASP, which act as a membrane tether [51]. Here, we showed that the property of stabilizing membrane domains through specific interactions with a membrane component is common to any protein surface and to different lipid compositions, being dictated solely by the partition properties of the protein–tether complex. Actin networks were also shown to serve as a membrane domain switch, as they drove membrane domain formation in otherwise homogeneous vesicles [51]. This behavior depends on the proximity to the critical point as the membrane becomes very sensitive to external perturbations [52]. It is possible that phase separation in homogeneous lipid mixtures, driven by interaction of membrane tethers with protein surfaces, is also a common occurrence in the vicinity of the critical point. In this case, immobilization of GUVs might drive segregation of membrane components even in the absence of phase coexistence. These phenomena are likely to be of great relevance not only for cytoskeleton driven membrane compartmentalization in living cells, but also for plasma membrane signalling mechanisms, which depend on major localized spatial and temporal changes in membrane composition, with the creation of signalling platforms with a specific set of components. The trigger to the formation of these platforms is typically the sequestration of specific membrane components upon a stimulus, generally the recognition of a ligand. In this way, interaction of a protein coated surface with segregated membrane tethers mimics this process, as changes in the distribution of one membrane component present at an extremely low density induces striking changes in the lateral distribution of all membrane components.

6. Conclusions

The use of GUVs in confocal/single-molecule studies of membrane phase coexistence is often performed through immobilization of the vesicles on a solid support. We showed here that as a consequence of differential partition to lipid phases, the membrane tethers used for immobilization have the potential to drastically change the distribution of lipid components within the vesicle, and in some conditions, a lipid phase was completely entrapped in the adherent area. This effect was particularly relevant for lipid mixtures presenting large domain areas, while lipid mixtures with smaller domains exhibited a lower degree of lipid domain reorganization.

On the light of these results, characterization of membrane phase separation on a single hemisphere is not able to fully characterize lipid phase coexistence, unless a membrane tether is used with no preferential partition to the lipid domains present in the vesicles. As a consequence of a partition coefficient close to unity, immobilization of GUVs presenting liquid ordered/liquid disordered phase coexistence with DPPE-biotin, did not result in significant reorganization of lipid domains within the GUVs, and despite relatively lower avidin binding affinity, this membrane tether should be preferentially used for studies on GUVs presenting these two lipid phases.

In addition, we showed that the property of stabilizing membrane domains through specific interactions with a membrane component is common to any protein surface and to different lipid compositions, being dictated solely by the partition properties of the protein–tether complex.

Acknowledgements

M.J.S. and F.F. acknowledge research grants (SFRH/BD/80575/2011 and SFRH/BPD/64320/2009) from Fundacão para a Ciência e Tecnologia (FCT). Authors acknowledge funding by FCT project references PTDC/QUI-BIQ/099947/2008, PTDC/QUI-BIQ/112067/2009, and PTDC/QUI-BIQ/119494/2010.

References

[1] B.M. Castro, L.C. Silva, A. Fedorov, R.F.M. de Almeida, M. Prieto, Cholesterol-rich fluid membranes solubilize ceramide domains: implications for the structure and dynamics of mammalian intracellular and plasma membranes, J. Biol. Chem. 284 (2009) 22978–22987.

[2] L.A. Bagatolli, To see or not to see: lateral organization of biological membranes and fluorescence microscopy, Biochim. Biophys. Acta 1758 (2006) 1541–1556.
[3] S.L. Veatch, S.L. Keller, Seeing spots: complex phase behavior in simple membranes, Biochim. Biophys. Acta 1746 (2005) 172–185.
[4] L. Guo, J.Y. Har, J. Sankaran, Y. Hong, B. Kannan, T. Wohland, Molecular diffusion measurement in lipid bilayers over wide concentration ranges: a comparative study, ChemPhysChem 9 (2008) 721–728.
[5] S.M. Christensen, D. Stamou, Surface-based lipid vesicle reactor systems: fabrication and applications, Soft Matter 3 (2007) 828.
[6] S. Ritz, K. Eisele, J. Dorn, S. Ding, D. Vollmer, S. Pütz, et al., Cationized albumin-biocoatings for the immobilization of lipid vesicles, Biointerphases 5 (2010) FA78–FA87.
[7] I. Stanish, J.P. Santos, A. Singh, One-step, chemisorbed immobilization of highly stable, polydiacetylenic phospholipid vesicles onto gold films, J. Am. Chem. Soc. 123 (2001) 1008–1009.
[8] S. Mourtas, M. Kastellorizios, P. Klepetsanis, E. Farsari, E. Amanatides, D. Mataras, et al., Covalent immobilization of liposomes on plasma functionalized metallic surfaces, Colloids Surf., B 84 (2011) 214–220.
[9] A. Percot, X.X. Zhu, M. Lafleur, Immobilization of lipid vesicles on polymer support via an amphiphilic peptidic anchor: application to a membrane enzyme, Bioconjugate Chem. 11 (2000) 674–678.
[10] H. Schönherr, D.I. Rozkiewicz, G.J. Vancso, Atomic force microscopy assisted immobilization of lipid vesicles, Langmuir 20 (2004) 7308–7312.
[11] L. Zhang, L. Hong, Y. Yu, S.C. Bae, S. Granick, Nanoparticle-assisted surface immobilization of phospholipid liposomes, J. Am. Chem. Soc. 128 (2006) 9026–9027.
[12] T.M. Hsin, K. Wu, G. Chellappan, Magnetically immobilized nanoporous giant proteoliposomes as a platform for biosensing, Analyst 137 (2012) 245–248.
[13] I. Kusters, N. Mukherjee, M.R. de Jong, S. Tans, A. Koçer, A.J.M. Driessen, Taming membranes: functional immobilization of biological membranes in hydrogels, PLoS One 6 (2011) e20435.
[14] R. Esquembre, S.N. Pinto, J.A. Poveda, M. Prieto, C.R. Mateo, Immobilization and characterization of giant unilamellar vesicles (GUVs) within porous silica glasses, Soft Matter 8 (2011) 408–417.
[15] C.H. Reccius, P. Fromherz, Giant lipid vesicles impaled with glass microelectrodes: GigaOhm seal by membrane spreading, Langmuir 20 (2004) 11175–11182.
[16] C. Yoshina-Ishii, S.G. Boxer, Arrays of mobile tethered vesicles on supported lipid bilayers, J. Am. Chem. Soc. 125 (2003) 3696–3697.
[17] S. Svedhem, I. Pfeiffer, C. Larsson, C. Wingren, C. Borrebaeck, F. Höök, Patterns of DNA-labeled and scFv-antibody-carrying lipid vesicles directed by material-specific immobilization of DNA and supported lipid bilayer formation on an Au/SiO2 template, ChemBioChem 4 (2003) 339–343.
[18] B.G. Lorz, A.S. Smith, C. Gege, E. Sackmann, Adhesion of giant vesicles mediated by weak binding of sialyl-Lewis X to E-selectin in the presence of repelling poly (ethylene glycol) molecules, Langmuir (2007) 12293–12300.
[19] T. Stora, Z. Dienes, H. Vogel, C. Duschl, Histidine-tagged amphiphiles for the reversible formation of lipid bilayer aggregates on chelator-functionalized gold surfaces, Langmuir 12 (2000) 5471–5478.
[20] S. Schuy, B. Treutlein, A. Pietuch, A. Janshoff, In situ synthesis of lipopeptides as versatile receptors for the specific binding of nanoparticles and liposomes to solid-supported membranes, Small 4 (2008) 970–981.
[21] L.S. Jung, J.S. Shumaker-Parry, C.T. Campbell, S.S. Yee, M.H. Gelb, Quantification of tight binding to surface-immobilized phospholipid vesicles using surface plasmon resonance: binding constant of phospholipase A2, J. Am. Chem. Soc. 122 (2000) 4177–4184.
[22] E. Boukobza, A. Sonnenfeld, G. Haran, Immobilization in surface-tethered lipid vesicles as a new tool for single biomolecule spectroscopy, J. Phys. Chem. B (2001) 12165–12170.
[23] D. Stamou, C. Duschl, E. Delamarche, H. Vogel, Self-assembled microarrays of attoliter molecular vessels, Angew. Chem. Int. Ed. Engl. 42 (2003) 5580–5583.
[24] P.D.J. Moens, E. Gratton, I.L. Salvemini, Fluorescence correlation spectroscopy, raster image correlation spectroscopy, and number and brightness on a commercial confocal laser scanning microscope with analog detectors (Nikon C1), Microsc. Res. Tech. 388 (2010) 377–388.
[25] M. Fidorra, A. Garcia, J.H. Ipsen, S. Härtel, L.A. Bagatolli, Lipid domains in giant unilamellar vesicles and their correspondence with equilibrium thermodynamic phases: a quantitative fluorescence microscopy imaging approach, Biochim. Biophys. Acta 1788 (2009) 2142–2149.
[26] R.F.M. de Almeida, J. Borst, A. Fedorov, M. Prieto, A.J.W.G. Visser, Complexity of lipid domains and rafts in giant unilamellar vesicles revealed by combining imaging and microscopic and macroscopic time-resolved fluorescence, Biophys. J. 93 (2007) 539–553.
[27] S.N. Pinto, L.C. Silva, R.F.M. de Almeida, M. Prieto, Membrane domain formation, interdigitation, and morphological alterations induced by the very long chain asymmetric C24:1 ceramide, Biophys. J. 95 (2008) 2867–2879.
[28] R. Haugland, Handbook of fluorescence probes and research chemicals, Molecular Probes, Eugene, OR , 1996.
[29] L.A. Sklar, B.S. Hudson, M. Petersen, J. Diamond, Conjugated polyene fatty acids as fluorescent probes: spectroscopic characterization, Biochemistry 16 (1977) 813–819.
[30] C. Boucheny, G.P. Bonneau, J. Droulez, G. Thibault, S. Ploix, A perceptive evaluation of volume rendering techniques, ACM Trans. Appl. Percept. 5 (2009) 1–24.
[31] L.C. Silva, R.F.M. de Almeida, B.M. Castro, A. Fedorov, M. Prieto, Ceramide-domain formation and collapse in lipid rafts: membrane reorganization by an apoptotic lipid, Biophys. J. 92 (2007) 502–516.
[32] L.A. Bagatolli, E. Gratton, Two-photon fluorescence microscopy observation of shape changes at the phase transition in phospholipid giant unilamellar vesicles, Biophys. J. 77 (1999) 2090–2101.
[33] N. Santos, Quantifying molecular partition into model systems of biomembranes: an emphasis on optical spectroscopic methods, Biochim. Biophys. Acta 1612 (2003) 123–135.
[34] L. Davenport, R.E. Dale, R.H. Bisby, R.B. Cundallt, Transverse location of the fluorescent probe 1,6-diphenyl- 1,3,5-hexatriene in model lipid bilayer membrane systems by resonance excitation energy transfer, Biochemistry 24 (1985) 4097–4108.
[35] B.W. Van Der Meer, G. Coker III, S.Y. Simon Chen, Resonance energy transfer: theory and data, VCH Publishers, New York, 1994.
[36] L.M. Loura, A. Fedorov, M. Prieto, Resonance energy transfer in a model system of membranes: application to gel and liquid crystalline phases, Biophys. J. 71 (1996) 1823–1836.
[37] C. Reyes Mateo, A. Ulises Acuña, J.C. Brochon, Liquid-crystalline phases of cholesterol/lipid bilayers as revealed by the fluorescence of trans-parinaric acid, Biophys. J. 68 (1995) 978–987.
[38] L.M.S. Loura, F. Fernandes, M. Prieto, Membrane microheterogeneity: Förster resonance energy transfer characterization of lateral membrane domains, Eur. Biophys. J. 39 (2010) 589–607.
[39] M. Castanho, M. Prieto, A. Ulises Acuña, The transverse location of the fluorescent probe trans-parinaric acid in lipid bilayers, Biochim. Biophys. Acta 1279 (1996) 164–168.
[40] L. Pugliese, A. Coda, M. Malcovati, M. Bolognesi, Three-dimensional structure of the tetragonal crystal form of egg-white avidin in its functional complex with biotin at 2.7 A resolution, J. Mol. Biol. 231 (1993) 698–710.
[41] T.J. McIntosh, A. Vidal, S.A. Simon, Sorting of lipids and transmembrane peptides between detergent-soluble bilayers and detergent-resistant rafts, Biophys. J. 85 (2003) 1656–1666.
[42] S. Manley, M.R. Horton, S. Lecszynski, A.P. Gast, Sorting of streptavidin protein coats on phase-separating model membranes, Biophys. J. 95 (2008) 2301–2307.
[43] M.L. Schmidt, L. Ziani, M. Boudreau, J.H. Davis, Phase equilibria in DOPC/DPPC: conversion from gel to subgel in two component mixtures, J. Chem. Phys. 131 (2009) 175103.
[44] R.F.M. de Almeida, A. Fedorov, M. Prieto, Sphingomyelin/phosphatidylcholine/cholesterol phase diagram: boundaries and composition of lipid rafts, Biophys. J. 85 (2003) 2406–2416.
[45] N.F. Morales-Penningston, J. Wu, E.R. Farkas, S.L. Goh, T.M. Konyakhina, J.Y. Zheng, et al., GUV preparation and imaging: minimizing artifacts, Biochim. Biophys. Acta 1798 (2010) 1324–1332.
[46] M. Loose, P. Schwille, Biomimetic membrane systems to study cellular organization, J. Struct. Biol. 168 (2009) 143–151.
[47] M.J. Swamy, D. Marsh, Spin-label studies on the anchoring and lipid-protein interactions of avidin with N-biotinylphosphatidylethanolamines in lipid bilayer membranes, Biochemistry 36 (1997) 7403–7407.
[48] I. Levental, D. Lingwood, M. Grzybek, U. Coskun, K. Simons, Palmitoylation regulates raft affinity for the majority of integral raft proteins, Proc. Natl. Acad. Sci. U. S. A. 107 (2010) 22050–22054.
[49] T.Y. Wang, R. Leventis, J.R. Silvius, Partitioning of lipidated peptide sequences into liquid-ordered lipid domains in model and biological membranes, Biochemistry 40 (2001) 13031–13040.
[50] T. Baumgart, G. Hunt, E.R. Farkas, W.W. Webb, G.W. Feigenson, Fluorescence probe partitioning between Lo/Ld phases in lipid membranes, Biochim. Biophys. Acta 1768 (2007) 2182–2194.
[51] A.P. Liu, D. a Fletcher, Actin polymerization serves as a membrane domain switch in model lipid bilayers, Biophys. J. 91 (2006) 4064–4070.
[52] J. Ehrig, E.P. Petrov, P. Schwille, Near-critical fluctuations and cytoskeleton-assisted phase separation lead to subdiffusion in cell membranes, Biophys. J. 100 (2011) 80–89.